

Vortex solitons in quasi-phase-matched photonic crystals

Feiyan Zhao¹, Xiaoxi Xu¹, Hexiang He¹, Li Zhang¹, Yangui Zhou¹, Zhaopin Chen², Boris A. Malomed^{3,4}, and Yongyao Li^{1,5*}

¹*School of Physics and Optoelectronic Engineering, Foshan University, Foshan 528000, China*

²*Physics Department and Solid-State Institute, Technion, Haifa 32000, Israel*

³*Department of Physical Electronics, School of Electrical Engineering, Faculty of Engineering, Tel Aviv University, Tel Aviv 69978, Israel*

⁴*Instituto de Alta Investigación, Universidad de Tarapacá, Casilla 7D, Arica, Chile*

⁵*Guangdong-Hong Kong-Macao Joint Laboratory for Intelligent Micro-Nano Optoelectronic Technology, Foshan University, Foshan 528000, China*

We report solutions for stable compound solitons in a three-dimensional quasi-phase-matched photonic crystal with the quadratic ($\chi^{(2)}$) nonlinearity. The photonic crystal is introduced with a checkerboard structure, which can be realized by means of the available technology. The solitons are built as four-peak vortex modes of two types, rhombuses and squares (intersite- and onsite-centered self-trapped states, respectively). Their stability areas are identified in the system's parametric space (rhombuses occupy an essentially broader stability domain), while all bright vortex solitons are subject to strong azimuthal instability in uniform $\chi^{(2)}$ media. Possibilities for experimental realization of the solitons are outlined.

Quadratic ($\chi^{(2)}$) media provide a versatile platform for the creation of optical solitons [1, 2]. Unlike the self-focusing cubic ($\chi^{(3)}$) nonlinearity, which generates two-dimensional (2D) solitons that are subject to the instability driven by the critical collapse in this setting [3, 4], $\chi^{(2)}$ systems support stable 2D fundamental (zero-vorticity) solitons in free space [2, 5, 6]. Actually, the $\chi^{(3)}$ effect can be emulated in $\chi^{(2)}$ media by means of the cascading mechanism when the intensity of the light beam increases to ~ 10 GW/cm² [7, 8].

Unlike the fundamental 2D $\chi^{(2)}$ solitons, ones with embedded vorticity (alias vortex rings) exhibit strong azimuthal instability which splits the vortex rings into fragments [9–11], which makes stabilization of vortex solitons a fundamental problem [4]. Working in this direction, it was predicted [12, 13] and demonstrated experimentally [14] that families of stable 2D vortex solitons can be supported by the competition of $\chi^{(2)}$ and self-defocusing $\chi^{(3)}$ nonlinearities. In other settings, stability of solitary vortices is provided by competing nonlinearities of other types, such as cubic-quintic in various forms [15–23], cubic-quartic in 3D [24], and cubic times a logarithmic factor in 2D [25]. In the latter two cases, such combinations of nonlinear terms model the competition of mean-field and beyond-mean-field interactions in binary Bose-Einstein condensates [26, 27]. Recently, stable vortex dissipative solitons have been predicted in a pure $\chi^{(2)}$ medium, by adding ring-shaped gain to the spatially uniform lossy background [28].

Designing new setups admitting stability of vortex solitons in $\chi^{(2)}$ media remains a relevant problem – in particular, because this may open a way for the creation of robust vortex rings using low-power optical beams. In this work, we propose a new possibility: stabilization of

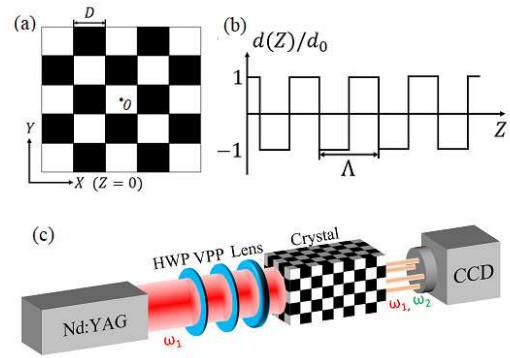


FIG. 1: (a) The checkerboard structure representing the nonlinear lattice in the input plane ($Z = 0$) as per Eq. (3). Black and white color cells correspond to $\sigma(X, Y) = 1$ and -1 , respectively. (b) The modulation of $d(Z)$, at a fixed point, where $\sigma(X, Y) = +1$ (black color cells), along the propagation distance with period Λ . (c) A schematic of the proposed experimental setup.

vortex rings by means of quasi-phase matching (QPM) nonlinear photonic crystals. By itself, QPM is a well-known method for achieving accurate phase matching in $\chi^{(2)}$ crystals for the nonlinear frequency conversion [29] in various settings [30]. This technique is based on spatial modulation of the $\chi^{(2)}$ susceptibility, imposed by means of periodic poling of the crystalline material [31–33] in 1D/2D and the femtosecond laser engineering technology in 3D [34–37], while the linear susceptibility is kept constant. Generally, there are three parameters of the QPM structure: the modulation period, duty cycle, and phase shift [38]. A periodically distributed phase shift creates a nonlinear lattice, alias a nonlinear photonic crystal [39].

We here elaborate a mechanism for the stabilization of vortex solitons by a 3D QPM nonlinear photonic crys-

*Electronic address: yongyaoli@gmail.com

tal. The paraxial propagation of light along direction Z is governed by coupled equations for the slowly varying fundamental-frequency (FF) and second-harmonic (SH) amplitudes, A_1 and A_2 :

$$i\partial_Z A_1 = -\frac{1}{2k_1}\nabla^2 A_1 - \frac{2d(X, Y, Z)\omega_1}{cn_1}e^{-i\Delta k Z} A_1^* A_2, \quad (1)$$

$$i\partial_Z A_2 = -\frac{1}{2k_2}\nabla^2 A_2 - \frac{d(X, Y, Z)\omega_2}{cn_2}e^{i\Delta k Z} A_1^2, \quad (2)$$

where $\nabla^2 = \partial_X^2 + \partial_Y^2$ is the paraxial-diffraction operator, c is the speed of light in vacuum, $k_{1,2}$, $\omega_{1,2}$ ($\omega_2 = 2\omega_1$), and $n_{1,2}$ are, respectively, the FF and SH carrier wavenumbers, frequencies, and refractive indices, with the phase mismatch $\Delta k = 2k_1 - k_2$. Further, the 3D periodically modulated local $\chi^{(2)}$ susceptibility is determined by $d(X, Y, Z) = \sigma(X, Y)d(Z)$, with a checkerboard structure in the (X, Y) plane:

$$\sigma(X, Y) = -\text{sgn}\{\cos(\pi X/D)\cos(\pi Y/D)\}, \quad (3)$$

where $D \times D$ is the size of each square cell, as shown in Fig. 1(a) (a 1D version of this pattern was considered to spatial control of entangled two-photon states, in Ref. [40]), and $d(Z) = d_0 \text{sgn}[\cos(2\pi Z/\Lambda)]$ is modulation function along the propagation distance, as shown in Fig. 1(b), which can be represented by its Fourier expansion corresponding to modulation period Λ :

$$d(Z) = d_0 \sum_{m \neq 0} \frac{2}{\pi m} \sin\left(\frac{\pi m}{2}\right) \exp\left(i\frac{2\pi m Z}{\Lambda}\right), \quad (4)$$

where d_0 corresponds to the coefficient $\chi^{(2)}$ and the respective duty cycle is $1/2$ [38]. We retain, as usual, a truncated form of expansion (4), with only the fundamental harmonics corresponding to $m = 1$ and $m = -1$ kept in Eqs. (1) and (2), respectively, as they play the dominant role in QPM.

Natural rescaling (cf. Ref. [41, 42]),

$$I_0 = \left(\frac{n_1}{\omega_1} + \frac{n_2}{\omega_2}\right) |A_0|^2, \quad z_d^{-1} = \frac{2d_0\omega_1}{\pi cn_1} \sqrt{\frac{\omega_2}{n_2}} I_0, \quad (5)$$

$$\psi_p = A_p \sqrt{\frac{n_p}{\omega_p I_0}} \exp[i(\Delta k - 2\pi/\Lambda)Z], \quad p = 1, 2, \quad (6)$$

$$z = Z/z_d, \quad x = X\sqrt{k_1/z_d}, \quad y = Y\sqrt{k_1/z_d}, \quad (7)$$

$$\Omega = z_d(\Delta k - 2\pi/\Lambda), \quad (8)$$

where A_0 is a characteristic amplitude of the electromagnetic field, and Ω is the effective detuning, casts Eqs. (1) and (2), with the truncated form of expansion (4), in the normalized form, with neglected difference between n_1 and n_2 (which is relevant for available materials):

$$i\partial_z \psi_1 = -\frac{1}{2}\nabla_{x,y}^2 \psi_1 - \Omega \psi_1 - 2\sigma(x, y)\psi_1^* \psi_2, \quad (9)$$

$$i\partial_z \psi_2 = -\frac{1}{4}\nabla_{x,y}^2 \psi_2 - \Omega \psi_2 - \sigma(x, y)\psi_1^2, \quad (10)$$

and $\nabla_{x,y}^2 = \partial_x^2 + \partial_y^2$. Equations (9) and (10) conserve two dynamical invariants, *viz.*, the total Hamiltonian and power (alias the Manley-Rowe invariant [43]),

$$H = \iint (\mathcal{H}_P + \mathcal{H}_\Omega + \mathcal{H}_{\chi^{(2)}}) dx dy \quad (11)$$

$$P = \iint (|\psi_1|^2 + 2|\psi_2|^2) dx dy \equiv P_1 + P_2. \quad (12)$$

where $\mathcal{H}_P = \frac{1}{2}|\nabla\psi_1|^2 + \frac{1}{4}|\nabla\psi_2|^2$, $\mathcal{H}_\Omega = -\Omega(|\psi_1|^2 + |\psi_2|^2)$, and $\mathcal{H}_{\chi^{(2)}} = -\sigma(x, y)[(\psi_1^*)^2 \psi_2 + \text{c.c.}]$. Power sharing between the FF and SH components is characterized by ratio $\gamma = P_2/P_1$. Control parameters of the resulting system are P , Ω , and D .

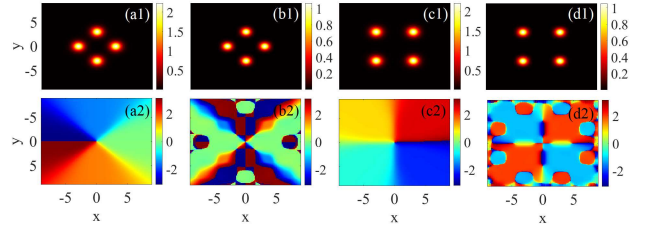


FIG. 2: Generic examples of stable rhombus-shaped and square-shaped vortex solitons composed of four peaks subject to condition $\varphi_2 = 2\varphi_1$ or $\varphi_2 = 2\varphi_1 - \pi$, respectively. These modes are centered at a white square cell, as shown in Fig. 1(a). Panels (a1,b1) and (c1,d1) display the distribution of the local intensity of the FF and SH components of the rhombus- and square-shaped vortex solitons, respectively. Panels (a2-d2) present the phase distribution of the solitons corresponding to (a1-d1), respectively. The parameters here are $(P, D, \Omega) = (40, 3, 0)$.

Bright-vortex soliton solutions to Eqs. (9) and (10) are looked for as

$$\psi_p(x, y, z) = \phi_p(x, y) \exp(ip\beta z), \quad p = 1, 2, \quad (13)$$

where $\phi_{1,2}$ represent the stationary shape of the FF and SH components, with propagation constants β and 2β , respectively. The $\chi^{(2)}$ terms in Eqs. (9) and (10) impose the matching condition on phases $\varphi_{1,2}(x, y) = \text{Arg}\{\phi_{1,2}(x, y)\}$ of the stationary solution:

$$\varphi_2(x, y) = 2\varphi_1(x, y) - \varphi_d(x, y), \quad (14)$$

where $\varphi_d(x, y)$ is decided by $\sigma(x, y)$. $\sigma(x, y) = 1$ and -1 correspond to $\varphi_d(x, y) = 0$ and π , respectively. It implies that there may exist two different types of the vortex solitons. Each one is built, essentially, of four peaks (local intensity maxima), which form rhombic or square patterns, as shown in Fig. 2. In these patterns, the vorticity is represented by the phase circulation along a closed path linking the peaks, which is the generic method for creating the multi-peak vortices supported by underlying lattice structures [44, 45] (the vorticity may be defined in this way even if the spatially modulated system does not conserve the angular momentum). As a

result, the rhombic and square-shaped patterns obey the matching condition (14) with $\varphi_2(x, y) = 2\varphi_1(x, y)$ or $\varphi_2(x, y) = 2\varphi_1(x, y) - \pi$. The matching condition does not hold in the empty square cell at the center of the rhombic pattern, hence this pattern may be classified as *intersite-centered* one [46], while the cell at the square's center may satisfy the matching, but is left empty, thus representing an *onsite-centered* self-trapped state. Accordingly, the rhombuses and squares are built, respectively, as densely and loosely packed structures.

Thus, the phase patterns of the two-component vortex solitons demonstrate, in Figs. 2(a2,c2), that the FF field carries the vorticity with winding number 1. As concerns the SH component, its phase is plotted in panels (b2,d2) on scale $-2\pi < \varphi_2 < +2\pi$, subtracting $\pm 2\pi$ in the region where Eq. (14) yields $|\varphi_2| > 2\pi$. For this reason, the phase patterns in these panels seem as corresponding to a quadrupole mode. Numerical results also demonstrate that, unlike previously studied multi-peak vortex solitons supported by linear square-shaped potentials [4, 44, 45], the present patterns are very sharp ones, in the sense that they do not feature side peaks in lattice cells which do not belong to the main rhombus or square. This feature may be useful for potential applications.

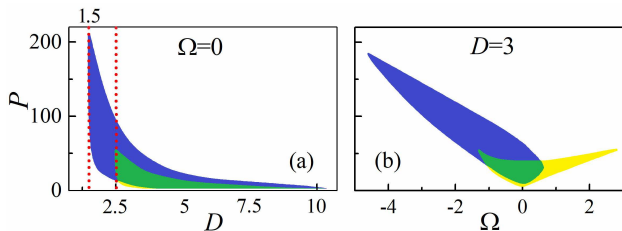


FIG. 3: The rhombic and square-shaped vortex solitons are stable, separately, in blue and yellow areas in the (P, D) parameter plane with $\Omega = 0$ (a), and in the (P, Ω) plane with $D = 3$ (b). They coexist as stable states in green areas in both planes. Vertical red dotted lines in (a) designate existence boundaries for the two soliton species.

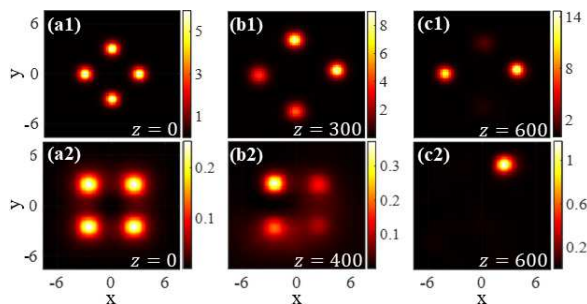


FIG. 4: Typical examples of the evolution of unstable solitons, which are selected outside of the stability area in Fig. 3. (a): Intensity shapes of unstable rhombic and square vortex solitons with $(P, D, \Omega) = (70, 3, 0)$ and $(5, 5, 0)$, plotted at $z = 0$ (a1,a2), 300 and 400 (b1,b2), and 600 (c1,c2), respectively.

Stability of the vortex solitons was verified by direct

simulations of the perturbed evolution in the framework of Eqs. (9) and (10), up to $z = 1000$. The resulting stability areas in the (P, D) and (P, Ω) planes are displayed in Fig. 3. Comparison of the results for the two types of the vortex solitons shows that the rhombic species has a wider stability area than its square-shaped counterpart. The difference is explained by the fact that the above-mentioned tight structure of the rhombuses helps to stabilize them stronger than it is possible with the help of the loose binding in squares. Indeed, the solitons of the former type remain stable up to value $P_{\max} \approx 200$ of the total power, while the square-shaped family has $P_{\max} \approx 60$. Intervals of the detuning parameter for the stable rhombuses and squares are, respectively, $-4.6 < \Omega < 0.6$ and $-1.3 < \Omega < 2.8$. Furthermore, there is a minimum size of spatial period D of the checkerboard lattice necessary for supporting rhombuses and squares, *viz.*, $D_{\min}^{(\text{rhomb})} = 1.5$ and $D_{\min}^{(\text{square})} = 2.5$, as shown by the vertical dotted red lines in Fig. 3(a). The compound vortex solitons do not exist at $D < D_{\min}$, as the rapid alternation of the sign in front of the $\chi^{(2)}$ terms in Eqs. (9) and (10) leads to effective cancellation of the quadratic nonlinearity. At $D > D_{\min}$, those rhombic and square-shaped solitons which are unstable spontaneously decay into sets of one or two peaks, as shown in Fig. 4.

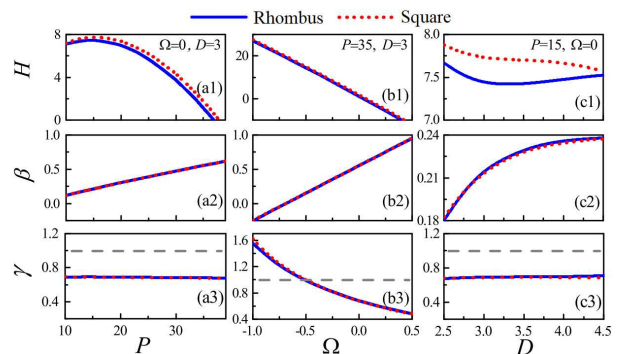


FIG. 5: Hamiltonian H , propagation constant β , and SH/FF power ratio γ for the vortex-soliton families vs. total power P , mismatch Ω , and spatial period D of the underlying lattice. The horizontal dashed lines in the bottom panels designate the level of $\gamma = 1$. Solid and dotted curves represent the rhombic- and square-shaped solitons, respectively. Parameters are fixed as $(\Omega, D) = (0, 3)$, $(P, D) = (35, 3)$, and $(P, \Omega) = (15, 0)$ in the left, middle, and right columns of panels, respectively. At these parameters, the curves in all the panels belong to the stability areas, see Fig. 3.

Families of the vortex solitons considered here are quantified by dependences of their characteristics, H , β , and γ , on P , Ω and D , as shown in Fig. 5. In particular, the top row shows that the rhombic solitons realize the system's ground state, as their value of the Hamiltonian is lower than that of the square-shaped ones. This property explains why the rhombuses have larger stability areas in Fig. 3. Further, Fig. 5(a2) shows that the soliton families satisfy the Vakhitov-Kolokolov criterion,

$d\beta/dP > 0$, which is a well-known necessary stability condition for solitons in self-focusing media [47]. The bottom row in Fig. 5 shows that the power-ratio factor γ depends solely on mismatch Ω , but not on P and D . Furthermore, Fig. 5(b3) shows that $\Omega = -0.5$ is a boundary between the two-component vortex solitons dominated by the SH and FF components (i.e., $\gamma > 1$ and $\gamma < 1$) at $\Omega < -0.5$ and $\Omega > -0.5$, respectively.

To verify the experimental feasibility of the present setup, the creation of stable two-component vortex solitons from the natural input in the form of the standard Laguerre-Gaussian vortex beam with winding number 1, initially launched into the checkerboard photonic crystal with length $z = 200$ in the FF component, was simulated too. Figure 6 shows a typical example, which demonstrates the formation of the well-defined soliton after passing $z \approx 8$. Naturally, the distance necessary for the creation of the robust output decreases with the increase of the input power. A schematic diagram of the experimental setup in which the above results may be realized is displayed above in Fig. 1(d). We also attempted to construct vortex-soliton solutions with winding number 2 in the FF component. However, the numerical analysis has not produced any such stable solutions [48].

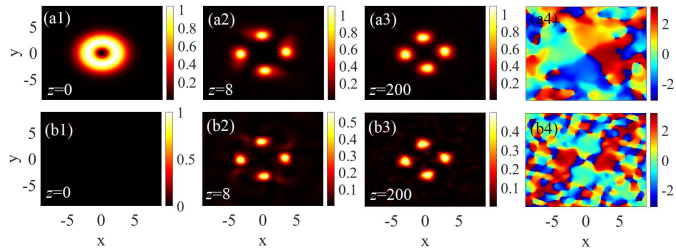


FIG. 6: The simulated propagation of the input launched in the FF component at $z = 0$ in the form a Laguerre-Gaussian vortex beam with $P = 40$ and winding number 1. (a1-a3) and (b1-b3): The intensity pattern of the FF and SH components are displayed at $z = 0$ (a1,b1), 8 (a2,b2) and 200 (a3,b3), respectively. (a4,b4): The FF phase pattern of FF and SH components at $z = 200$, respectively. Here, $D = 3$ and $\Omega = 0$ are fixed.

To estimate experimentally relevant characteristics for the predicted compound solitons, we adopt parameters for lithium niobate ($d_0 = 27$ pm/V [49], $n_1 \approx n_2 \approx 2.2$). Experimentally relevant values of the FF and SH wavelengths, and amplitude of the electric field A_0 in Eq. (5) are chosen as 1064 nm and 532 nm, and 200 kV/cm [2], respectively, which yields the propagation-distance scale $z_d = 0.0625$ cm [cf. Eq. (5)]. Table I summarizes relations between the variables in the scaled and physical units.

With the values from Table I, the total power for the solitons displayed in Fig. 2 is 1600 W, peak intensities of both components being ≈ 0.17 GW/cm². The physical propagation length corresponding to $z = 1000$ is 62.5 cm, which is tantamount to hundreds of the Rayleigh (diffrac-

TABLE I: The relation between the coordinates, intensities, and power measured in scaled and physical units.

$z = 1$ & $\Omega = 1$	0.0625 cm & 16 cm ⁻¹
$x = 1$ & $y = 1$	7 μ m
$ \psi_1 ^2 = 1$ & $ \psi_2 ^2 = 1$	80 MW/cm ² & 160 MW/cm ²
$P = 1$	40 W

tion) lengths, corroborating the complete stability of the solitons. We also note that, because the $\chi^{(3)}$ coefficient for the same material is 36.6×10^{-22} m²/V² [50], the Kerr nonlinearity is indeed negligible in the present setting for the current soliton intensity. Further, the spatial period of the checkerboard in the range of $1.5 \leq D \leq 10$ corresponds to the width of the square cell ranging from 10 μ m to 70 μ m in physical units. In particular, zero mismatch, $\Omega = 0$, is attained at $\Lambda \approx 6.65$ μ m (the refractive index difference for the FF and SH components with the type-I polarization is $\Delta n \approx 0.08$ [51], producing, as mentioned above, a negligible effect in the present setup). These length scales are realistic for the implementation using the available QPM-fabrication technique. In physical units, Fig. 6 demonstrates that the input in the form of the Laguerre-Gaussian vortex beam with power 1600 W and FWHM width 20 μ m the soliton is formed at $Z \approx 0.5$ cm (which corresponds to the scaled distance $z \approx 8$). The respective experimental setup is shown above in Fig. 1(d). The appropriate Laguerre-Gaussian laser beam at wavelength $\lambda = 1064$ nm can be generated by a high-power laser source, e.g., a Nd:YAG system generating pulses with energy and temporal width 10 μ J and 6 ns, at 40 Hz repetition rate. The half-wavelength plane (HWP), adjusted to the type-I polarization type, and the vortex-phase plates (VPP) morph the input into a vortex beam with orbital angular momentum $l = 1$, which is focused by the lens onto the photonic crystal. Then, it evolves as shown in Fig. 6. According to the above estimates, the optical multi-peak vortex soliton can be generated and detected by the CCD in the output beam, provided that the crystal's length exceed 0.5 cm.

Losses of the optical medium may be considered as well. According to Refs. [52], we assume that the loss rate for both FF and SH waves in lithium niobate is $\approx 1.56\%$ per centimeter. Adding the linear losses to Eqs. (9) and (10), we have checked that the system still predicts the formation of robust vortex solitons. For example, the rhombic and square-shaped solitons observed at $Z = 20$ cm keep more than 70% of the initial power.

In conclusion, we have produced two families of compound vortex solitons, rhombic and square-shaped ones (which are intersite- and onsite-centered self-trapped states, respectively), in the $\chi^{(2)}$ medium equipped with the QPM checkerboard lattice. Unlike completely unstable vortex solitons in spatially uniform $\chi^{(2)}$ systems, the presently considered families feature broad stability areas in the system's parameter space. The tightly-bound

rhombic vortex solitons realize the system's ground state, featuring the lowest value of the Hamiltonian and a larger stability area than loosely bound squares. Physical characteristics of the predicted vortex-soliton families belong to the range accessible to currently available experimental techniques.

The analysis can be extended in other directions. In particular, a natural objective is to consider a chirped QPM, corresponding to Z/Λ replaced by $\int dZ/\Lambda(Z)$ in Eq. (4), with variable spatial period $\Lambda(Z)$, which makes detuning Ω a function of Z in Eq. (8) and suggests possibilities to manipulate the solitons, cf. Ref. [53]. On the other hand, if the Fourier components with $|m| > 1$ are taken into account, an effective cubic nonlinearity with self- and cross-phase modulation can be induced through the cascading mechanism. It may also be relevant to include the intrinsic $\chi^{(3)}$ nonlinearity into the consideration. Effects of the cubic terms on the stability of vortex solitons is an interesting issue [13, 54]. A challenging problem is mobility of 2D vortex solitons against the lattice backdrop. Previously, mobility was demon-

strated only for fundamental 2D lattice solitons in the $\chi^{(2)}$ system [55].

Acknowledgments

This work was supported by the NNSFC (China) through Grants No. 12274077, 11874112, 11905032, 62005044, by the Guangdong Basic and Applied Basic Research Foundation through grant No. 2021A1515111015, the Key Research Projects of General Colleges in Guangdong Province through grant No. 2019KZDXM001, the Research Fund of Guangdong-Hong Kong-Macao Joint Laboratory for Intelligent Micro-Nano Optoelectronic Technology through grant No. 2020B1212030010 and the Graduate Innovative Talents Training Program of the Foshan University. The work of B.A.M. is supported, in part, by the Israel Science Foundation through grant No. 1695/22.

-
- [1] C. Etrich, F. Lederer, B. A. Malomed, T. Peschel, and U. Peschel, Optical solitons in media with a quadratic nonlinearity, *Progress in Optics* **41**, 483-568 (2000).
- [2] A. V. Buryak, P. D. Trapani, D. V. Skryabin, and S. Trillo, Optical solitons due to quadratic nonlinearities: from basic physics to futuristic applications, *Phys. Rep.* **370**, 63-235 (2002).
- [3] G. Fibich, *The Nonlinear Schrödinger Equation: Singular Solutions and Optical Collapse* (Springer, Cham, 2015).
- [4] B. A. Malomed, *Multidimensional Solitons* (AIP Publishing, Melville, New York, 2022).
- [5] W. E. Torruellas, Z. Wang, D. J. Hagan, E. W. VanStryland, G. I. Stegeman, L. Torner, and C. R. Menyuk, Observation of Two-Dimensional Spatial Solitary Waves in a Quadratic Medium, *Phys. Rev. Lett.* **74**, 5036 (1995).
- [6] W. E. Torruellas, Z. Wang, L. Torner, and G. I. Stegeman, Observation of mutual trapping and dragging of two-dimensional spatial solitary waves in a quadratic medium, *Opt. Lett.* **20**, 1949 (1995).
- [7] R. DeSalvo, D. J. Hagan, M. Sheik-Bahae, G. Stegeman, and E. W. Van Stryland, Self-focusing and self-defocusing by cascaded second-order effects in KTP, *Opt. Lett.* **17**, 28 (1992).
- [8] Ch. Bosshard, R. Spreiter, M. Zgonik, and P. Günter, Kerr Nonlinearity via Cascaded Optical Rectification and the Linear Electro-optic Effect, *Phys. Rev. Lett.* **74**, 2876 (1995).
- [9] W. J. Firth and D. V. Skryabin, Optical solitons carrying orbital angular momentum, *Phys. Rev. Lett.* **79**, 2450-2453 (1997).
- [10] L. Torner and D. V. Petrov, Azimuthal instabilities and self-breaking of beams into sets of solitons in bulk second-harmonic generation, *Electronics Lett.* **33**, 608-610 (1997).
- [11] D. V. Petrov, L. Torner, J. Martorell, R. Vilaseca, J. P. Torres, and C. Cojocar, Observation of azimuthal modulational instability and formation of patterns of optical solitons in a quadratic nonlinear crystal, *Opt. Lett.* **23**, 1444-1446 (1998).
- [12] I. Towers, A. V. Buryak, R. A. Sammut, and B. A. Malomed, Stable localized vortex solitons, *Phys. Rev. E* **63**, 055601(R) (2001).
- [13] D. Mihalache, D. Mazilu, B. A. Malomed, F. Lederer, Stable vortex solitons supported by competing quadratic and cubic nonlinearities. *Phys. Rev. E.* **69**, 066614 (2004).
- [14] P. D. Trapani, W. Chinaglia, S. Minardi, A. Piskarskas, and G. Valiulis, Observation of quadratic optical vortex solitons, *Phys. Rev. Lett.* **84**, 3843 (2000).
- [15] M. Quiroga-Teixeiro and H. Michinel, Stable azimuthal stationary state in quintic nonlinear optical media, *J. Opt. Soc. Am. B* **14**, 2004-2009 (1997).
- [16] V. I. Berezhiani, V. Skarka, and N. B. Aleksić, Dynamics of localized and nonlocalized optical vortex solitons in cubic-quintic nonlinear media, *Phys. Rev. E* **64**, 057601 (2001).
- [17] D. Mihalache, D. Mazilu, L.-C. Crasovan, I. Towers, A. V. Buryak, B. A. Malomed, L. Torner, J. P. Torres, and F. Lederer, Stable spinning optical solitons in three dimensions, *Phys. Rev. Lett.* **88**, 073902 (2002).
- [18] R. L. Pego and H. A. Warchall, Spectrally stable encapsulated vortices for nonlinear Schrödinger equations, *J. Nonlin. Science* **12**, 347-394 (2002).
- [19] D. Mihalache, D. Mazilu, F. Lederer, Y. V. Kartashov, L.-C. Crasovan, L. Torner, and B. A. Malomed, Stable vortex tori in the three-dimensional cubic-quintic Ginzburg-Landau equation. *Phys. Rev. Lett.* **97**, 073904 (2006).
- [20] J. M. Soto-Crespo, N. Akhmediev, C. Mejía-Cortés, and N. Devine, Dissipative ring solitons with vorticity, *Opt. Exp.* **17**, 4236-4250 (2009).
- [21] C. Mejía-Cortés and J. M. Soto-Crespo, Vortex solitons of the discrete Ginzburg-Landau equation, *Phys. Rev. A* **83**, 043837 (2011).

- [22] C. Cartes, J. Cisternas, O. Descalzi, and H. R. Brand, Model of a two-dimensional extended chaotic system: Evidence of diffusing dissipative solitons, *Phys. Rev. Lett.* **109**, 178303 (2012).
- [23] Y. Y. Wang, L. Chen, C. Q. Dai, J. Zheng, and Y. Fan, Exact vector multipole and vortex solitons in the media with spatially modulated cubic-quintic nonlinearity, *Nonlin. Dynamics* **90**, 1269-1275 (2017).
- [24] Y. V. Kartashov, B. A. Malomed, L. Tarruell, and L. Torner, Three-dimensional droplets of swirling superfluids, *Phys. Rev. A*, **98**, 013612 (2018).
- [25] Y. Li, Z. Chen, Z. Luo, C. Huang, H. Tan, Wei Pang, and Boris A. Malomed, Two-dimensional vortex quantum droplets, *Phys. Rev. A* **98**, 063602 (2018).
- [26] D. S. Petrov, Quantum mechanical stabilization of a collapsing Bose-Bose mixture, *Phys. Rev. Lett.* **115**, 155302 (2015).
- [27] D. S. Petrov and G. E. Astrakharchik, Ultradilute low-dimensional liquids, *Phys. Rev. Lett.* **117**, 100401 (2016).
- [28] V. E. Lobanov, A. A. Kalinovich, O. V. Borovkova, B. A. Malomed, Fundamental and vortex dissipative quadratic solitons supported by spatially localized gain. *Phys. Rev. A* **105**, 013519 (2022)
- [29] A. Arie, and N. Voloch, Periodic, quasi-periodic, and random quadratic nonlinear photonic crystals, *Laser and Photonic Rev.* **4**, 355 (2010).
- [30] H. Li and B. Ma, Research development on fabrication and optical properties of nonlinear photonic crystals, *Front. Optoelectronics* **13**, 35 (2020).
- [31] M. Houe and P. D. Townsend, An introduction to method of periodic poling for 2nd-harmonic generation, *J. Phys. D – Appl. Phys.*, **28**, 1747-1763 (1995).
- [32] T. Hatanaka, K. Nakamura, T. Taniuchi, H. Ito, Y. Furukawa, and K. Kitamura, Quasi-phase-matched optical parametric oscillation with periodically poled stoichiometric LiTaO₃, *Opt. Lett.* **25**, 651-653 (2000).
- [33] A. Chowdhury, H. M. Ng, M. Bhardwaj, and N. G. Weimann, Second-harmonic generation in periodically poled GaN, *Appl. Phys. Lett.* **83**, 1077-1079 (2003).
- [34] T. Xu, K. Switkowski, X. Chen, S. Liu, K. Koynov, H. Yu, H. Zhang, J. Wang, Y. Sheng, and W. Krolikowski, Three-dimensional nonlinear photonic crystal in ferroelectric barium calcium titanate, *Nature Photonics* **12**, 591 (2018).
- [35] D. Wei, C. Wang, H. Wang, X. Hu, D. Wei, X. Fang, Y. Zhang, D. Wu, Y. Hu, J. Li, S. Zhu, and M. Xiao, Experimental demonstration of a three-dimensional lithium niobate nonlinear photonic crystal, *Nature Photonics* **12**, 596 (2018).
- [36] S. Keren-Zur, and T. Ellenbogen, A new dimension for nonlinear photonic crystals, *Nat. Photonics*, **12**, 575 (2018).
- [37] A. Arie, Storing and retrieving multiple images in 3D nonlinear photonic crystals, *Light: Science & application*, **10**, 202 (2021).
- [38] A. Karniel, and A. Arie, Fully controllable adiabatic geometric phase in nonlinear optics, *Opt. Exp.* **26**, 4920 (2018).
- [39] M. Skorobogatiy and J. Yang, *Fundamentals of Photonic Crystal Guiding* (Cambridge University Press, Cambridge, 2009).
- [40] J. P. Torres, A. Alexandrescu, S. Carrasco, and L. Torner, Quasi-phase-matching engineering for spatial control of entangled two-photon states, *Opt. Lett.* **29**, 376 (2004).
- [41] C. R. Phillips, C. Langrock, D. Chang, Y. W. Lin, L. Gallmann, and M. M. Fejer, Apodization of chirped quasi-phases-matching devices, *J. Opt. Soc. Am. B* **30**, 1551 (2013).
- [42] F. Zhao, J. Lü, H. HE, Y. Zhou, S. Fu, and Y. Li, Geometric phase with full-wedge and half-wedge rotation in nonlinear frequency conversion, *Opt. Exp.* **29**, 21820 (2021).
- [43] G. Porat, and A. Arie, Efficient, broadband, and robust frequency conversion by fully nonlinear adiabatic three-wave mixing, *J. Opt. Soc. Am. B* **30**, 1342 (2013).
- [44] B. B. Baizakov, B. A. Malomed, and M. Salerno, Multidimensional solitons in periodic potentials, *Europhys. Lett.* **63**, 642-648 (2003).
- [45] J. Yang and Z. H. Musslimani, Fundamental and vortex solitons in a two-dimensional optical lattice, *Opt. Lett.* **28**, 2094-2096 (2003).
- [46] B. A. Malomed and P. G. Kevrekidis, Discrete vortex solitons, *Phys. Rev. E* **64**, 026601 (2001).
- [47] N. G. Vakhitov and A. A. Kolokolov, Stationary solutions of the wave equation in a medium with nonlinearity saturation, *Radiophys. Quantum Electron.* **16**, 783-789 (1973); <https://doi.org/10.1007/BF01031343>.
- [48] Additional numerical results demonstrate that modes with a quadrupole structure (instead of the vortex) in the FF component exist and some of them are stable.
- [49] 27 pm/V is the largest value of the lithium niobate's nonlinear tensor, d_{33} . Generally, $d_0 = (2/\pi)d_{33}$. In Eq. (5), the coefficient of $(2/\pi)$ is separated, hence we set $d_0 = d_{33}$ in this paper. [http://en.wikipedia.org/wiki/Lithium_niobate]
- [50] I. A. Kulagin, R. A. Ganeev, V. A. Kim, A. I. Rysanyansky, R. I. Tugushev, T. Usmanov, A. V. Zinoviev, Nonlinear refractive indices and third-order susceptibilities of nonlinear-optical crystals, *Proc. SPIE 4972, Nonlinear Frequency Generation and Conversion: Materials, Devices, and Applications II* (2003).
- [51] D. H. Jundt, Temperature-dependent Sellmeier equation for the index of refraction, n_e , in congruent lithium niobate, *Opt. Lett.* **22**, 1553 (1997).
- [52] T. Kashiwazaki, T. Yamashima, N. Takanashi, A. Inoue, T. Umeki, and A. Furusawa, Fabrication of low-loss quasi-single-mode PPLN waveguide and its application to a modularized broadband high-level squeezer, *Appl. Phys. Lett.* **119**, 251104 (2021).
- [53] A. Karnieli, Y. Li, and A. Arie, The geometric phase in nonlinear frequency conversion, *Front. Phys.* **17**, 12301 (2022).
- [54] C. B. Clausen, O. Bang, and Y. S. Kivshar, Spatial Solitons and Induced Kerr Effects in Quasi-Phase-Matched Quadratic Media, *Phys. Rev. Lett.* **78**, 4749 (1997).
- [55] H. Susanto, P. G. Kevrekidis, R. Carretero-Gonzalez, B. A. Malomed, and D. J. Frantzeskakis, Mobility of discrete solitons in quadratically nonlinear media. *Phys. Rev. Lett.* **99**, 214103 (2007).